Mode switch based on electro-optic long-period waveguide grating in lithium niobate

Jin, Wei; Chiang, Kin Seng

Published in:
Optics Letters

Published: 15/01/2015

Document Version:
Post-print, also known as Accepted Author Manuscript, Peer-reviewed or Author Final version

Publication record in CityU Scholars:
Go to record

Published version (DOI):
10.1364/OL.40.000237

Publication details:
Jin, W., & Chiang, K. S. (2015). Mode switch based on electro-optic long-period waveguide grating in lithium niobate. *Optics Letters*, *40*(2), 237-240. Advance online publication. https://doi.org/10.1364/OL.40.000237

Mode switch based on electro-optic long-period waveguide grating in lithium niobate

Wei Jin and Kin Seng Chiang,*

Department of Electronic Engineering, City University of Hong Kong, 83 Tat Chee Avenue, Kowloon, Hong Kong, China
**Corresponding author: eeksc@cityu.edu.hk*

Received Month X, XXXX; revised Month X, XXXX; accepted Month X, XXXX; posted Month X, XXXX (Doc. ID XXXXX); published Month X, XXXX

We propose a mode switch based on an electro-optic long-period grating formed in a lithium-niobate (LN) two-mode waveguide. Our fabricated device consists of an 8-mm-long grating in a proton-exchanged *z*-cut LN waveguide. At a driving voltage of 35 V, it can switch between the fundamental mode and the higher-order mode with a mode extinction ratio of –18 dB and a 3-dB bandwidth of ~25 nm at the wavelength 1544 nm. The performance of the device is insensitive to temperature variations. The experimental results agree well with the simulation. This mode switch could find applications in reconfigurable mode-division-multiplexing systems.

OCIS Codes: (050.2770) Gratings; (130.3730) Lithium niobate; (130.4815) Optical switching devices.
http://dx.doi.org/10.1364/OL.99.099999

Thanks to the continuous growth of the Internet traffic, it will not take long for the transmission capacity of optical communication systems based on single-mode fibers to reach its limit. Different technologies are being pursued worldwide to increase the transmission capacity of optical fiber links. Mode-division multiplexing (MDM) is one of the promising technologies and has attracted increasing attention [1–5]. In an MDM system, a few-mode fiber is used as the transmission medium, where different modes in the fiber carry different channels of signals. One of the basic components in an MDM system is a mode converter that converts the fundamental mode to a high-order mode and vice versa [1–16].

Mode converters can be realized with bulk-optic components [2–4], long-period fiber gratings [1,4,6–8], and optical waveguide devices, such as multimode interference couplers [9], asymmetric mode couplers [5,10], asymmetric Y junctions [11], and micro-ring resonators [12]. These mode converters can provide fixed mode conversion and are often used in conjunction with mode (de)multiplexers to facilitate connection with existing single-mode components. In a reconfigurable MDM system, where switching among the modes is necessary for signal routing, a switchable mode converter, or a mode switch, is needed. A mode switch in an MDM system plays the same role as a wavelength switch in a reconfigurable wavelength-division-multiplexing system. There are few mode switches developed for MDM applications. Switchable mode conversion has been demonstrated with an electromagnet-driven dynamic long-period grating along a two-mode fiber [13], but the setup is cumbersome. Mode switching can also be achieved by propagating an acoustic wave at a specific frequency along a two-mode fiber, but the bandwidth of such an acousto-optic grating is narrow and the converted mode is frequency-shifted [14]. Although the bandwidth of an acousto-optic grating can be significantly increased by using a specially designed hole-assisted fiber [15], the extinction ratio achieved is low and the use of a complex fiber structure also presents some practical difficulties. More recently, a polymer-waveguide mode switch based on an unbalanced Mach-Zehnder interferometer connected to a thermally controlled two-mode interferometer has been demonstrated [16], but the configuration of the device is complicated and the switching speed is slow. In this paper, we propose a fast, compact electro-optic (EO) waveguide mode switch for MDM applications.

Our proposed mode switch is implemented with a *z*-cut lithium-niobate (LN) two-mode waveguide that supports two transverse-magnetic (TM) modes, where the conversion between the two modes is controlled by an EO grating formed along the waveguide. To achieve effective coupling between these two modes, we employ a push-pull electrode structure for the generation of the EO grating. Our experimental device consists of an 8-mm-long EO grating along a proton-exchanged LN waveguide. At a driving voltage of 35 V, the device can achieve a maximum mode conversion efficiency of 98.5% (or a mode extinction ratio of –18 dB) at the wavelength 1544 nm with a 3-dB bandwidth of ~25 nm. The characteristics of the device are insensitive to temperature variations. We have previously demonstrated EO gratings in single-mode LN waveguides for the realization of tunable filters by coupling the core mode to a cladding mode [17, 18]. Compared with the cladding-mode EO grating filter, which is fabricated with a special two-step proton-exchange process [17, 18], the present mode switch has a simpler waveguide structure and can be fabricated with the much simpler conventional proton-exchange process.

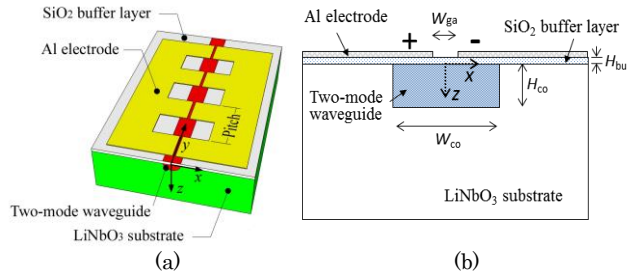

Fig. 1. (a) Schematic diagram of the EO waveguide mode switch and (b) the cross-section of the waveguide structure that assumes an effective step-index rectangular core.

Figure 1(a) shows a schematic diagram of the proposed EO mode switch, which consists of a proton-exchanged *z*-cut *y*-propagation LN two-mode waveguide, a thin SiO_2 buffer layer, and a periodic aluminum (Al) electrode. As the proton-exchange process increases only the extraordinary refractive index of the LN substrate, the waveguide supports only the TM modes: the TM_{00} mode (the fundamental mode) and the TM_{10} mode (the higher-order mode), which have symmetric and antisymmetric field distributions along the *x* direction, respectively. To allow the two modes to couple to each other efficiently, we employ a push-pull electrode structure to exploit the largest EO coefficient r_{33} of the LN crystal, where the electrodes are placed on top of the waveguide and separated by a small gap at the center of the waveguide, as shown in Fig. 1. When a voltage is applied across the electrodes, one side of the waveguide experiences an increase in the refractive index, while the other side experiences a decrease, which thus leads to an antisymmetric EO induced index distribution and hence a superposition of the EO effects from the two sides of the waveguide.

We fabricated the device with the following steps. We first deposited a 100-nm-thick chromium (Cr) film on the surface of a 15 × 10 × 0.5 mm (width × length × thickness) *z*-cut LN substrate by radio-frequency (RF) sputtering and then opened a set of 4.5-μm-wide channels with a separation of 60 μm on the Cr film by the standard photolithography process. We submerged the patterned sample into the proton source stearic acid at 250 °C for 90 min, which resulted in an array of waveguide cores. With the Cr mask removed, the sample was annealed in a convection oven at 300 °C for 16 hours. With the availability of an array of identical channel waveguides, we were able to measure the effective index of the channel waveguide with a prism-coupler system (Metricon, Model 2010) [19]. The waveguide supported only the TM_{00} and TM_{10} modes at the wavelength 1536 nm and their measured effective indices were N_{00} = 2.1456 and N_{10} = 2.1403, respectively. We next deposited a 0.2-μm-thick SiO_2 buffer layer on the surface of the waveguide channels by RF sputtering, which served to isolate the waveguides from the electrode.

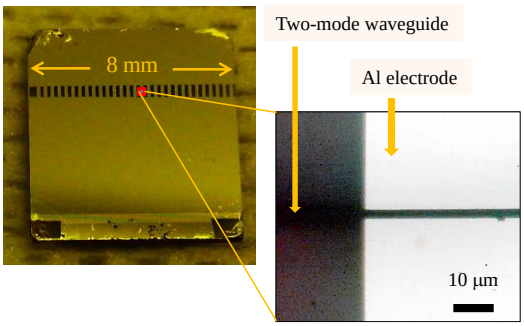

Fig. 2. Photograph of the sample with the magnified view showing the positions of the two-mode waveguide and the Al electrode.

According to the phase-matching condition, the pitch of the electrode grating is given by $\Lambda = \lambda_0/(N_{01} - N_{11})$, where λ_0 is the resonance wavelength at which the coupling between the two modes is strongest. With the knowledge of N_{00} and N_{10}, the grating pitch was estimated to be 293 μm at the wavelength 1550 nm. To form the electrode structure, we deposited a 100-nm-thick Al film on top of the SiO_2 buffer layer by RF sputtering and then processed the Al film by standard photolithography. The actual grating pitch used in our sample was 295 μm, which is somewhat longer than the calculated value to take into account the effect of the SiO_2 buffer layer on the effective indices. The grating length was 8 mm. Although a number of channel waveguides were formed in the substrate for the sake of measuring the effective indices, only one channel waveguide was covered with the electrode. Figure 2 is a photograph of the fabricated device, where the magnified view shows the relative positions of the waveguide and the electrode. As shown in Fig. 2, the electrode gap, which is about 3 μm, is well aligned with the center of the waveguide. We polished both ends of the waveguide and used lens fibers to launch and collect light to/from the waveguide.

The transmission spectra of the TM_{00} mode was measured with a broadband source (ALS-15CL, Amonics) and an optical spectrum analyzer (AQ6370, Yokogawa) at different driving voltages at the temperature 26 °C when only the TM_{00} mode was excited are shown in Fig. 3(a). A rejection band is clearly present in the transmission spectrum, which is caused by the coupling of the TM_{00} mode to the TM_{10} mode. The contrast of the rejection band increases with the driving voltage up to a certain value and a further increase in the voltage results in over-coupling and hence a reduction in the contrast. A maximum contrast of ~18 dB at 1544 nm is achieved at a driving voltage of 35 V (the half-π voltage), which corresponds to a mode conversion efficiency of 98.5%. The 3-dB bandwidth of the rejection band at 35 V is ~25 nm.

To confirm that the rejection band shown in Fig. 3(a) was indeed due to the expected mode conversion, we launched only the TM_{00} mode into the waveguide at the wavelength 1544 nm and captured the near-field images

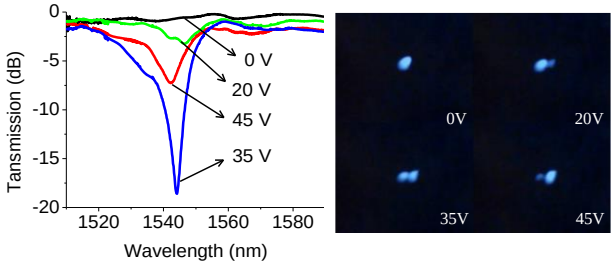

Fig. 3. (a) Normalized transmission spectra of the TM_{00} mode of the mode switch measured at different driving voltages at the temperature 26 °C. (b) Output near-field images taken at different driving voltages.

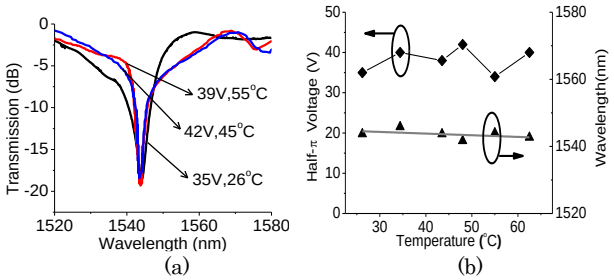

Fig. 4. (a) Normalized transmission spectra of the TM_{00} mode of the mode switch measured at different temperatures and the corresponding half-π voltages. (b) Change of the half-π voltage and the resonance wavelength of the mode switch with the temperature.

of the output light with an infrared camera. The results are shown in Fig. 3(b). At 0 V, the output from the waveguide is the pure TM_{00} mode. At 20 V, the output image consists of a mix of the TM_{00} mode and the TM_{10} mode. At 35 V, practically only the TM_{10} mode appears at the output. At 45 V, the image shows a mix of the two modes again. These results confirm strong coupling from the TM_{00} mode to the TM_{10} mode at 35 V. We also monitored the total output power from the waveguide, as we varied the driving voltage. We observed no significant change in the output power, which indicates negligible power loss to radiation modes. The spot size of the TM_{00} mode (defined at 1/e of the peak intensity) was measured to be 8.5 × 5.6 μm (width × height). The loss of the TM_{00} mode, measured by the transmission method at 1550 nm [20], was ~0.8 dB/cm.

We also measured the change of the transmission spectrum with the temperature by using a hot plate placed at the bottom of the device. As shown by the results in Fig. 4, the resonance wavelength and the half-π voltage are insensitive to the temperature change over the range from 26 to 63 °C. The temperature sensitivity of the resonance wavelength is lower than –0.05 nm/°C. This weak temperature dependence can be attributed to the fact that both modes propagate in same core area and, therefore, experience almost equal thermally induced changes in the effective indices.

To verify the experiment results, we analyze the performance of the mode switch with the coupled-mode theory. According to the coupled-mode theory, the transmission spectrum of the TM_{00} mode is given by

$$T(\lambda) = 1 - \frac{\kappa^2}{\kappa^2 + \frac{\delta^2}{4}} \sin^2 \sqrt{\kappa^2 + \frac{\delta^2}{4}} L \qquad (1)$$

with

$$\delta = \frac{2\pi}{\lambda}(N_{00} - N_{10}) - \frac{2\pi}{\Lambda} \qquad (2)$$

where λ is the operation wavelength, L is the grating length, and κ is the coupling coefficient. The coupling coefficient κ measures the spatial overlap between the two coupled modes over the grating area [18]:

$$\kappa = \frac{n_{su}}{\lambda c \mu_0} \int_{-\infty}^{+\infty} \int_{-\infty}^{+\infty} \left[-\frac{1}{2} n_{su}^3 r_{33}(x,z) V F(x,z) \right] \vec{E}_{00} \vec{E}_{10} \, dxdz \qquad (3)$$

where n_{su} is the substrate index, c is the speed of light in vacuum, μ_0 is the permeability, $r_{33}(x,z)$ is the EO coefficient of the LN waveguide, V is the driving voltage, $F(x,z)$ is the z component of the electric-field distribution produced by the electrode across the waveguide at V= 1 V, and $\vec{E}_{00}(x,z)$ and $\vec{E}_{10}(x,z)$ are the normalized electric fields of the TM_{00} and TM_{10} modes, respectively.

We calculate the electric-field distribution $F(x, z)$ with a commercial electrostatic solver (RSoft Design Group), where the electrode thickness is neglected and the static relative permittivity values of air (1.0), SiO_2 (3.9), and LN (84 in the x direction and 28 in the z direction) are assumed [18]. The gap between the electrodes is W_{ga} = 3μm. Thanks to the push-pull electrode structure, the electric-field distribution $F(x,z)$ and hence the EO induced index change is antisymmetric with respect to x = 0. As the TM_{10} mode field is also antisymmetric with respect to x = 0, the EO effects from the two sides of the electrode structure contribute equally to the coupling efficient.

We model the refractive-index profile of the LN waveguide with an effective step-index profile [18] – see Fig. 1(b). From the spot size and the effective index of the TM_{00} mode (measured, respectively, from the near-field image and the prism-coupler system), the width W_{co} and the height H_{co} of the effective step-index core are determined to be 4.0 μm and 6.45 μm, respectively, and the refractive indices of the core and the substrate are n_{co} = 2.1528 and n_{su} = 2.138, respectively. The thickness of the SiO_2 buffer is H_{bu} = 0.2 μm. Using these parameters, we calculate the field distributions of the two TM modes with a mode solver (FIMMWAVE, Photon Design) and the results at the wavelength 1544 nm are shown in Fig. 5(a). The calculated effective indices of the TM_{00} and TM_{10} mode are 2.14561 and 2.14032, respectively, and the pitch of the grating required is 292 μm, which is close to the value used in the experiments. The EO coefficient r_{33} is equal to 30.8 pm/V (for a bulk LN crystal at 1550 nm) in the substrate and 85% of that value in the core, which takes into account the loss of the EO strength

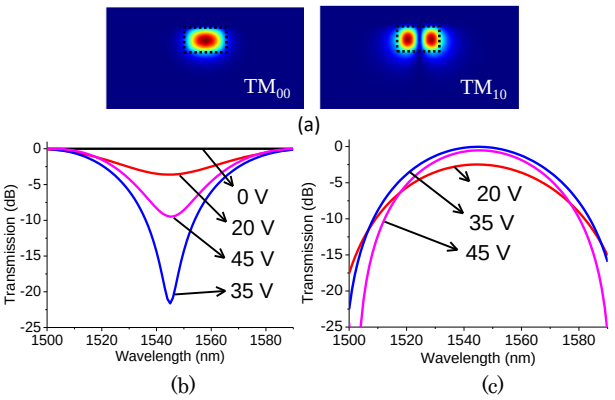

Fig. 5. (a) Calculated intensity patterns of the two TM modes supported by the waveguide at the wavelength 1544 nm. Transmission spectra of (b) the TM_{00} mode and (c) the TM_{10} mode of the device calculated for different driving voltages, assuming that only the TM_{00} mode is launched into the waveguide.

in the proton-exchange process and the partial recovery of the EO strength in the post-annealing process [18].

Assuming that only the TM_{00} mode is launched into the waveguide, we calculate the transmission spectra of the TM_{00} and TM_{10} modes for different driving voltages and show the results in Fig. 5(b) and (c), respectively. When a driving voltage is applied, a rejection band (pass band) appears in the TM_{00} (TM_{10}) spectrum at the wavelength 1544 nm. The contrast of the rejection band reaches its maximum value at ~35 V. As the voltage continues to increase, the contrast decreases, as a result of over-coupling (i.e., the TM_{10} mode is coupled back to the TM_{00} mode). The 3-dB bandwidth of the rejection band at 35 V is ~40 nm. The simulation agrees reasonably well with the experiment results. We should note that, in the case that only the TM_{10} mode is launched into the waveguide, Fig. 5(b) and (c) represent the transmission spectra of the TM_{10} and TM_{00} modes, respectively.

In conclusion, we have experimentally demonstrated a mode switch with an 8-mm-long EO grating formed on an annealed proton-exchanged LN two-mode waveguide. This mode switch is capable of converting the TM_{00} mode to the TM_{10} mode at a driving voltage of 35 V with a mode extinction ratio of –18 dB (or a mode conversion efficiency of 98.5%) at 1544 nm. The 3-dB bandwidth of the mode conversion is ~25 nm. It should be possible to reduce the half-π voltage to less than 10 V by increasing the length of the grating and improving the electrode design. It should also be possible to apply the same principle to higher-order modes by using proper electrode configurations and grating pitches appropriate to the waveguide design. While our specific design is based a proton-exchanged LN waveguide, the design approach and methodology can certainly be applied to other types of LN waveguides, such as Ti or Zn in-diffusion LN waveguides. Our EO mode switch has potential applications in reconfigurable MDM communication systems.

This work was supported by a grant from the Research Grants Council of the Hong Kong SAR, China, under Project CityU 112113.

References

1. Y. Jung, S. U. Alam, Z. Li, A. Dhar, D. Giles, I. P. Giles, J. K. Sahu, F. Poletti, L. Grüner-Nielsen, and D. J. Richardson, Opt. Express **19**, B952–B957 (2011).
2. R. Ryf, S. Randel, A. H. Gnauck, C. Bolle, A. Sierra, S. Mumtaz, M. Esmaeelpour, E. C. Burrows, R.-J. Essiambre, P. J. Winzer, D. W. Peckham, A. H. McCurdy, and R. Lingle Jr., J. Lightw. Technol. **30**, 521 (2012).
3. V. A. J. M. Sleiffer, Y. Jung, V. Veljanovski, R. G. H. van Uden, M. Kuschnerov, H. Chen, B. Inan, L. Grüner-Nielsen, Y. Sun, D. J. Richardson, S. U. Alam, F. Poletti, J. K. Sahu, A. Dhar, A. M. J. Koonen, B. Corbett, R. Winfield, A. D. Ellis, and H. de Waardt, Opt. Express **20**, B428 (2012).
4. A. Li, X. Chen, A. Al Amin, J. Ye, and W. Shieh, J. Lightw. Technol. **30**, 3953–3964 (2012).
5. N. Hanzawa, K. Saitoh, T. Sakamoto, T. Matsui, K. Tsujikawa, M. Koshiba, and F. Yamamoto, Opt. Express **21**, 25752–25760 (2013)
6. C. D. Poole, H. M. Presby, and J. P. Meester, Electron. Lett. **30**, 1437 (1994).
7. S. Ramachandran, Z. Wang, and M. Yan, Opt. Lett. **27**, 698 (2002).
8. I. Giles, A. Obeysekara, R. Chen, D. Giles, F. Poletti, and D. Richardson, IEEE Photon. Technol. Lett. **24**, 1922 (2012).
9. J. Leuthold, R. Hess, J. Eckner, P. A. Besse, and H. Melchior, Opt. Lett. **21**, 836 (1996).
10. Y. Ding, J. Xu, F. Da Ros, B. Huang, H. Ou, and C. Peucheret, Opt. Express **21**, 10376 (2013).
11. J. B. Driscoll, R. R. Grote, B. Souhan, J. I. Dadap, M. Lu, and R. M. Osgood Jr., Opt. Lett. **38**, 1854 (2013).
12. L.-W. Luo, N. Ophir, C. P. Chen, L. H. Gabrielli, C. B. Poitras, K. Bergmen, and M. Lipson, Nat. Commun. **5**, 3069 (2014).
13. H. Sakata, H. Sano, and T. Harada, Opt. Fiber Technol. **20**, 224 (2014).
14. H. S. Kim, S. H. Yun, I. K. Kwang, and B. Y. Kim, Opt. Lett. **22**, 1476 (1997).
15. T. Matsui, K. Nakajima, K. Shiraki, and T. Kurashima, J. Lightw. Technol. **27**, 2183 (2009).
16. W. Y. Chan, and H. P. Chan, Opt. Express **22**, 9282 (2014).
17. W. Jin, K. S. Chiang, and Q. Liu, Opt. Express, **16**, 20409 (2008).
18. W. Jin, K. S. Chiang, and Q. Liu, IEEE J. Lightw. Technol. **28**, 1477 (2010).
19. K. S. Chiang and S. Y. Cheng, Opt. Eng. **47**, 034601(1-4) (2008).
20. W. J. Wang, S. Honkanen, S. I. Najafi, and A. Tervonen, J. Appl. Phys. **74**, 1529 (1993).

Full References:

1. Y. Jung, S. U. Alam, Z. Li, A. Dhar, D. Giles, I. P. Giles, J. K. Sahu, F. Poletti, L. Grüner-Nielsen, and D. J. Richardson, "First demonstration and detailed characterization of a multimode amplifier for space division multiplexed transmission systems," Opt. Express 19, B952–B957 (2011).
2. R. Ryf, S. Randel, A. H. Gnauck, C. Bolle, A. Sierra, S. Mumtaz, M. Esmaeelpour, E. C. Burrows, R.-J. Essiambre, P. J. Winzer, D. W. Peckham, A. H. McCurdy, and R. Lingle Jr., "Mode-division multiplexing over 96 km of few-mode fiber using coherent 6 × 6 MIMO processing," J. Lightw. Technol. 30, 521–531 (2012).
3. V. A. J. M. Sleiffer, Y. Jung, V. Veljanovski, R. G. H. van Uden, M. Kuschnerov, H. Chen, B. Inan, L. Grüner-Nielsen, Y. Sun, D. J. Richardson, S. U. Alam, F. Poletti, J. K. Sahu, A. Dhar, A. M. J. Koonen, B. Corbett, R. Winfield, A. D. Ellis, and H. de Waardt, "73.7Tb/s (96x3x256-Gb/s) mode-division-multiplexed DP-16QAM transmission with inline MM-EDFA," Opt. Express 20, B428–B438 (2012).
4. A. Li, X. Chen, A. Al Amin, J. Ye, and W. Shieh, "Space-Division Multiplexed High-speed superchannel transmission over few-mode fiber," J. Lightw. Technol. 30, 3953–3964 (2012).
5. N. Hanzawa, K. Saitoh, T. Sakamoto, T. Matsui, K. Tsujikawa, M. Koshiba, and F. Yamamoto, "Two-mode PLC-based mode multi/demultiplexer for mode and wavelength division multiplexed transmission," Opt. Express 21, 25752–25760 (2013).
6. C. D. Poole, H. M. Presby, and J. P. Meester, "Two-mode fiber spatial-mode converter using periodic core deformation," Electron. Lett. 30, 1437–1438 (1994).
7. S. Ramachandran, Z. Wang, and M. Yan, "Bandwidth control of long-period grating-based mode converters in few-mode fibers," Opt. Lett. 27, 698–700 (2002).
8. I. Giles, A. Obeysekara, R. Chen, D. Giles, F. Poletti, and D. Richardson, "Fiber LPG mode converters and mode selection technique for multimode SDM," IEEE Photon. Technol. Lett. 24, 1922–1925 (2012).
9. J. Leuthold, R. Hess, J. Eckner, P. A. Besse, and H. Melchior, "Spatial mode filters realized with multimode interference couplers," Opt. Lett. 21, 836–838 (1996).
10. Y. Ding, J. Xu, F. Da Ros, B. Huang, H. Ou, and C. Peucheret, "On-chip two-mode division multiplexing using tapered directional coupler-based mode multiplexer and demultiplexer," Opt. Express 21, 10376–10382 (2013).
11. J. B. Driscoll, R. R. Grote, B. Souhan, J. I. Dadap, M. Lu, and R. M. Osgood Jr., "Asymmetric Y junctions in silicon waveguides for on-chip mode-division multiplexing," Opt. Lett. 38, 1854–1856 (2013).
12. L.-W. Luo, N. Ophir, C. P. Chen, L. H. Gabrielli, C. B. Poitras, K. Bergmen, and M. Lipson, "WDM-compatible mode-divsion multiplexing on a silicon chip," Nat. Commun. 5, 3069 (2014).
13. H. Sakata, H. Sano, and T. Harada, "Tunable mode converter using electromagnet-induced long-period grating in two-mode fiber," Opt. Fiber Technol. 20, 224–227 (2014).
14. H. S. Kim, S. H. Yun, I. K. Kwang, and B. Y. Kim, "All-fiber acousto-optic tunable notch filter with electronically controllable spectral profile," Opt. Lett. 22, 1476–1478 (1997).
15. T. Matsui, K. Nakajima, K. Shiraki, and T. Kurashima, "Ultra-Broadband Mode Conversion With Acousto-Optic Coupling in Hole-Assisted Fiber," J. Lightw. Technol. 27, 2183–2188 (2009).
16. W. Y. Chan, and H. P. Chan, "Reconfigurable two-mode mux/demux device," Opt. Express 22, 9282–9290 (2014).
17. W. Jin, K. S. Chiang, and Q. Liu, "Electro-optic long-period waveguide gratings in lithium niobate," Opt. Express, 16, 20409-20417 (2008).
18. W. Jin, K. S. Chiang, and Q. Liu, "Analysis of Lithium Niobate electrooptic long-period waveguide gratings," IEEE J. Lightw. Technol. 28, 1477-1484 (2010).
19. K. S. Chiang and S. Y. Cheng, "A technique of applying the prism-coupler method for accurate measurement of the effective indices of channel waveguides", Opt. Eng., 47, 034601(1-4) (2008).
20. W. J. Wang, S. Honkanen, S. I. Najafi, and A. Tervonen, "Loss characteristics of potassium and silver double-ion-exchanged glass waveguides," J. Appl. Phys., 74, 1529-1533 (1993).